Electronic structure of In_2O_3 and Sn-doped In_2O_3 by hard x-ray photoemission spectroscopy

C. Körber, V. Krishnakumar, and A. Klein
Darmstadt University of Technology, 64287 Darmstadt, Germany

G. Panaccione
Laboratorio TASC, INFM-CNR, Area Science Park, S.S. 14, Km 163.5, 34012 Trieste, Italy

P. Torelli
CNR-INFM-S3, Via Campi 213/A, I-41100 Modena, Italy

A. Walsh
Department of Chemistry, University College London, 20 Gordon Street, London WC1H, United Kingdom

J. L. F. Da Silva
Instituto de Fìsica de São Carlos, Universidade de São Paulo, Caixa Postal, 369, São Carlos 13560-970 SP, Brazil

S.-H. Wei
National Renewable Energy Laboratory, Golden, Colorado 80401, USA

R. G. Egdell and D. J. Payne
Department of Chemistry, Chemistry Research Laboratory, University of Oxford, Mansfield Road, Oxford OX1 3TA, United Kingdom
(Received 10 December 2009; revised manuscript received 15 March 2010; published 27 April 2010)

The valence and core levels of In_2O_3 and Sn-doped In_2O_3 have been studied by hard x-ray photoemission spectroscopy ($h\nu=6000$ eV) and by conventional Al Kα ($h\nu=1486.6$ eV) x-ray photoemission spectroscopy. The experimental spectra are compared with density-functional theory calculations. It is shown that structure deriving from electronic levels with significant In or Sn 5*s* character is selectively enhanced under 6000 eV excitation. This allows us to infer that conduction band states in Sn-doped samples and states at the bottom of the valence band both contain a pronounced In 5*s* contribution. The In 3*d* core line measured at $h\nu=1486.6$ eV for both undoped and Sn-doped In_2O_3 display an asymmetric lineshape, and may be fitted with two components associated with screened and unscreened final states. The In 3*d* core line spectra excited at $h\nu=6000$ eV for the Sn-doped samples display pronounced shoulders and demand a fit with two components. The In 3*d* core line spectrum for the undoped sample can also be fitted with two components, although the relative intensity of the component associated with the screened final state is low, compared to excitation at 1486.6 eV. These results are consistent with a high concentration of carriers confined close to the surface of nominally undoped In_2O_3. This conclusion is in accord with the fact that a conduction band feature observed for undoped In_2O_3 in Al Kα x-ray photoemission is much weaker than expected in hard x-ray photoemission.

DOI: 10.1103/PhysRevB.81.165207 PACS number(s): 71.20.Nr, 79.60.Bm, 73.20.At, 71.15.Mb

I. INTRODUCTION

Transparent conducting oxides (TCOs) combine the properties of optical transparency in the visible region with a high electrical conductivity. The most widely used TCOs are based on post-transition metal oxides such as ZnO, CdO, SnO_2, and In_2O_3. These oxides all have *optical* band gaps in excess of 3 eV and are therefore transparent to visible-light radiation. They are however amenable to degenerate *n* type doping, typically by replacement of the host cation by an element one group to the right in the periodic table. The onset of optical absorption is shifted to higher energies due to occupation of the conduction band (the Moss-Burstein shift)[1,2] and the material remains transparent down to the energy of the conduction electron plasmon, below which there is a high reflectivity. With carrier concentrations typically ranging from 10^{20} cm^{-3} to above 10^{21} cm^{-3}, plasmon energies up to about 1 eV are found. TCOs find a wide range of applications as transparent electrodes in flat panel displays,[3,4] organic light emitting diodes (OLEDs) (Ref. 5) and solar cells. They are also used in electrochromic devices, where the optical properties are modulated upon charge insertion/extraction to give so-called "smart windows."[3]

One of the most important TCOs is Sn-doped In_2O_3, widely known as ITO (indium tin oxide). Despite the importance of this material, the nature of the band gap in In_2O_3 itself has remained contentious. Measurements by Weiher and Ley[6] showed an onset of strong optical absorption at around 3.75 eV which was attributed to a direct allowed gap. However, a weaker onset at 2.62 eV was also observed and attributed to indirect transitions. Despite these observations, the band gap of In_2O_3 has been quoted to be around 3.7 eV in many hundreds of publications. The conduction band minimum for In_2O_3 is found at the Γ point and the indirect gap hypothesis therefore requires that there must be pronounced upward dispersion of the uppermost valence band away from Γ. Dispersion of this sort is found in CdO due to mixing between shallow core Cd 4*d* states and O 2*p* states.[7]

Within a centrosymmetric structure, mixing between states of different symmetry such as p and d is forbidden at the Γ point, but the parity restriction is relaxed away from Γ. However, theoretical work by Erhart *et al.*[8] showed that although the valence-band maximum was indeed displaced away from the Γ point, the upward dispersion was only around 50 meV. This is much too small to account for the large shift between the strong and weak absorption onsets observed by Weiher and Ley ($\sim$1 eV). X-ray emission spectroscopy confirms that the extent of mixing between In 4d and O 2p states in In_2O_3 is very much less pronounced than the shallow core mixing in CdO.[7,9]

More recent work based on x-ray spectroscopies, in conjunction with first-principle density-functional theory (DFT) calculations of the optical spectra, has resolved this controversey.[10,11] It has been found that transitions from all the states in the upper part of the valence band are either dipole forbidden, or carry very low dipole intensity, and there is a large shift between the forbidden onset of optical absorption and the effective optical gap of about 3.7 eV. In the fully ionic limit the valence band of In_2O_3 is of pure O 2p atomic character, while the lowest empty conduction-band states are of In 5s character. However, to fully understand the electronic structure in this important material it is important to be able to assess the extent of mixing between the valence orbitals of In and O in the valence and conduction bands. Of course band-structure calculations contain this information, but it is not trivial to confirm theoretical results with experiments which decompose the valence and conduction bands into component orbitals.

Historically x-ray photoemission spectroscopy (XPS), using either Al Kα or Mg Kα radiation, has been a workhorse technique for the study of filled states in solids. Valence-band XPS samples the whole Brillouin zone and there is little influence from final state effects. Thus, for noncorrelated materials the technique effectively probes the total density of states, weighted by cross sections for ionization of component orbitals. O K-shell x-ray emission (XES) has been shown to be very effective at elucidating the O 2p contribution to the valence-band states in oxides and experiments on In_2O_3 have been performed.[7,9] It is more problematic to obtain direct information about the metal ns orbital contribution to electronic states (where n is the principal quantum number). In principle decay into metal np core holes will sample the metal s and d partial densities of states but the In 4p and 5p levels suffer from pronounced lifetime broadening and x-ray emission involving decay into these levels is very weak and difficult to measure.[12–14]

We have recently shown that hard x-ray photoelectron spectroscopy (HAXPES) provides an approach to the study of the contribution of metal ns states to valence and conduction bands in simple oxides.[15–17] Final state wave functions for the high-energy photoelectrons produced in valence band HAXPES have a short characteristic wavelength and oscillate rapidly over the length range which characterizes the radial distribution of typical valence orbitals. However, the wave functions of ns orbitals with $n \geq 4$ are highly penetrating, with rapidly oscillating inner radial maxima whose length scale may better match the final state wave functions. Thus the inner part of the ns wave function provides a contribution to the dipole matrix elements that determine ionization cross sections, that decays less rapidly with increasing photon energy, than is typical for nonpenetrating orbitals such as O 2p. Thus the ns contribution to the partial density of states is selectively enhanced at high photon energies. In addition the inelastic electron mean free path increases with increasing electron kinetic energy so that HAXPES is very much less surface sensitive than conventional XPS.[18–25] We exploit both these aspects of the HAXPES technique in the current study of In_2O_3 and Sn-doped In_2O_3 thin films.

II. EXPERIMENTAL DETAILS

Nominally undoped In_2O_3 and Sn-doped In_2O_3 (2 and 10 weight% Sn) thin films were deposited by radio frequency magnetron sputtering onto doped Si substrates, to a thickness of 400 nm, using pure Ar as the sputter gas and a 400 °C substrate temperature.[26] The measured conductivities are 142 S/cm, 4185 S/cm, and 5998 S/cm for the undoped, 2% and 10% Sn-doped samples, respectively. Assuming a typical carrier mobility of 30 cm^2/Vs,[27] this translates to carrier concentrations of 3.0×10^{19}, 8.7×10^{20}, and 1.2×10^{21} cm^{-3}. A second series of samples were deposited on quartz substrates under identical conditions. The onsets of strong optical absorption for these samples were found at 3.71, 4.17, and 4.49 eV for the undoped, 2% and 10% Sn-doped In_2O_3, respectively.

High-resolution x-ray photoemission spectra were measured in a Scienta ESCA 300 spectrometer. This incorporates a rotating anode Al Kα ($h\nu$=1486.6 eV) x-ray source, a seven crystal x-ray monochromator and a 300 mm mean radius spherical sector electron energy analyzer with parallel electron detection system. The x-ray source was run with 200 mA emission current and 14 kV anode bias, while the analyzer operated at 150 eV pass energy with 0.8 mm slits. Gaussian convolution of the analyzer resolution with a linewidth of 260 meV for the x-ray source gives an effective instrument resolution of 400 meV. XPS spectra of the samples deposited on Si were also measured *in situ* in the deposition system. The integrated surface analysis and preparation system DAISY-MAT[28] includes a Physical Electronics PHI 5700 photoelectron spectrometer equipped with a monochromatic Al Kα x-ray source, an OMNI IV imaging lens system and a five channeltron electron detector. At 5.85 eV pass energy the overall resolution of the spectrometer, as determined from the Gaussian broadening of the Fermi edge of a sputter cleaned Ag sample, amounts to 350 meV.

Hard x-ray photoemission measurements at $h\nu$ =6000 eV were performed on beamline ID16 of the European Synchrotron Radiation Facility in Grenoble (France) using the VOLPE (volume photoemission) endstation.[22,29–31] The radiation from the undulator on beamline ID16 was linearly polarized in the horizontal plane and was incident at 45° to the sample surface. Photoelectrons were collected in normal emission in the horizontal plane, so that the angle between the offtake direction and both the propagation and polarization vectors of the beam was 45°. The effective beamline resolution was set at 300 meV at 6000 eV photon energy. The spectrometer resolution was set at 200 meV for

most measurements. The total overall energy resolution was 360 meV. The typical time for accumulation of In 3*d* core level spectra was 1 h, while valence-band spectra required longer accumulation times of around 4 h. No sample degradation was observed at higher photon energies.

III. THEORETICAL DETAILS

The electronic structures of In_2O_3 and Sn-doped In_2O_3 were calculated in the cubic bixbyite structure using DFT (Refs. 32 and 33) employing the all-electron projector augmented wave method[34] as implemented in the VASP code.[35,36] Exchange-correlation effects were treated within the generalized gradient approximation as formulated by Perdew, Burke, and Ernzerhof (PBE) functional.[37] A 500 eV cutoff for the plane-wave basis set was employed. Both the In and Sn $4d^{10}$ and O $2s^2$ states were treated explicitly as valence. For bulk In_2O_3 a full stress and volume minimization was performed using a higher plane-wave cutoff (700 eV) to avoid errors associated with Pulay stress, with the internal atomic positions relaxed until the forces on all atomic sites were below 0.005 eV/Å. The equilibrium PBE lattice constant was found to be $a=10.30$ Å, 1.8% greater than the experimental value (10.117 Å).[38] A well-converged $4\times4\times4$ Monkhorst-Pack[39] *k*-point grid was employed, with an increased density of $6\times6\times6$ used for calculation of the electronic density of states.

At the PBE level, the band gaps of insulators are underestimated, and this is the case for In_2O_3 with a calculated fundamental band gap of 1.22 eV.[11,40] However, if a nonlocal hybrid-DFT exchange-correlation functional is employed, where 25% of the short-range PBE exchange is replaced with exact exchange from Hartree-Fock theory (HSE06 functional),[41–44] we predict a band gap of 2.74 eV at the experimental lattice constant.[45] In comparison, the HSE03 functional, which features stronger screening of the nonlocal exchange, has been reported to predict a band gap of 2.45 eV.[46]

To deal with Sn doping, one In atom was replaced by Sn in the 80 atom In_2O_3 cell. This corresponds to replacement of 1 In atom in 32 i.e., 3.1% doping and a carrier concentration of 9.7×10^{20} cm^{-3}. The energetic difference between substitution on the 8*b* or 24*d* In sites is small (60 meV), with the trigonally distorted 8*b* octahedra favored; this is in agreement with analysis of Mössbauer spectra.[47] Differences in the resulting electronic structure are minor and results are presented for the lowest-energy 8*b* substitution. At this doping level, the system is found to be degenerate with the Fermi energy located within the In_2O_3 conduction band. For this case a $6\times6\times6$ *k*-point grid was used for accurate determination of the Fermi level position, with Brillouin zone integration performed using the tetrahedron method including Blöchl corrections.

IV. RESULTS AND DISCUSSION

A. Valence-band structure in photoemission

The valence- and conduction-band structures in x-ray photoemission spectra of In_2O_3, 2% and 10% ITO measured at excitation energies of 1486.6 and 6000 eV are shown in Fig. 1. For convenience of presentation the spectra are normalized to the maximum of intensity in the valence band. For the measurements carried out at $h\nu=1486.6$ eV the maximum intensity is found for component I, while for samples measured at $h\nu=6000$ eV the maximum intensity is found for component IV. The valence band of In_2O_3 is comprised of four main features labeled I, II, III, and IV, with peak maxima at 3.9, 5.3, 6.8, and 8.6 eV. For 2% and 10% ITO the peaks are shifted to higher binding energy and another feature V is seen at ~10.5 eV. The band-structure calculation shown in Figs. 2 and 3 for In_2O_3 and 3.1% ITO demonstrate that band I relates to states of predominant O 2*p* character. The O 2*p* contribution is around 90% but with some mixing with In 4*d* states. Bands II and III by contrast involve mixing between O 2*p* and In 5*p* orbitals, while states in band IV arise from strong In 5*s* and O 2*p* mixing. At the peak maximum in band IV the states have around 38% In 5*s* character and 62% O 2*p* character. For ITO, band V is of almost pure Sn 5*s* character. Under excitation at 1486.6 eV photon energy, band I is the strongest feature in the valence band, bands II and III are of intermediate intensity and band IV is the weakest feature of the spectrum. When the incident photon energy is increased to 6000 eV the relative intensity of bands III and IV relative to I and II increases dramatically and band IV becomes the strongest valence-band spectral feature. These striking changes arise from changes in the photoionization cross-sections for the orbitals involved in the

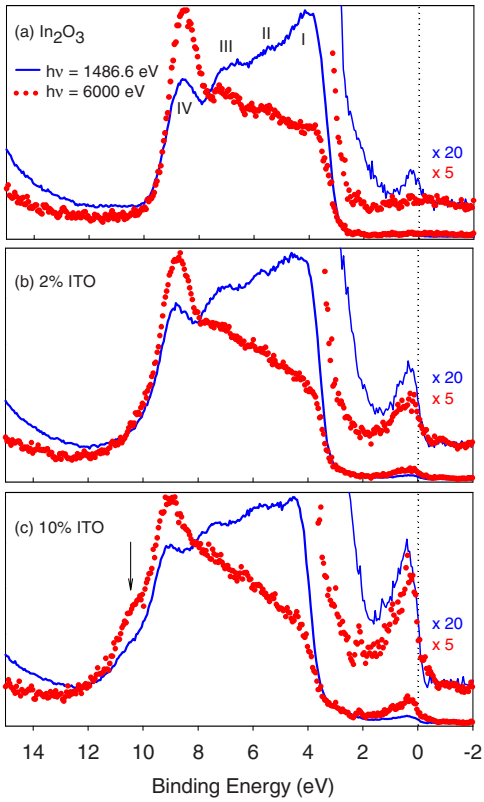

FIG. 1. (Color online) Valence- and conduction-band spectra of (a) In_2O_3, (b) 2% ITO, and (c) 10% ITO measured at 1486.6 and 6000 eV. Note: Expansion of conduction band ×20 for spectra measured at 1486.6 eV and ×5 for spectra measured at 6000 eV.

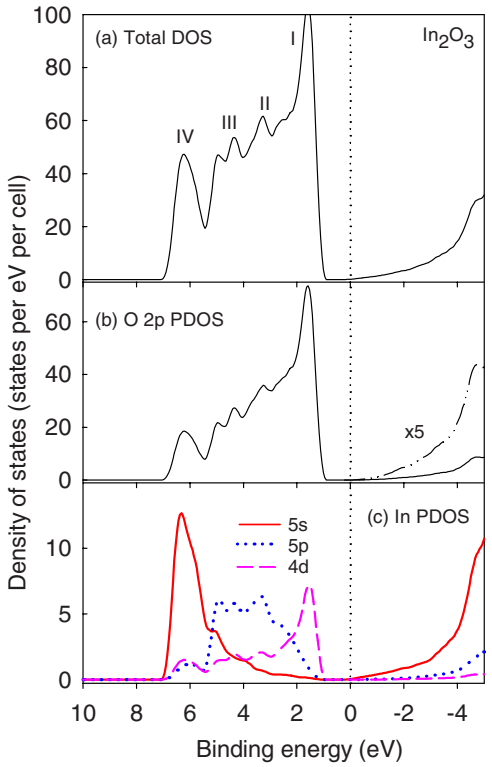

FIG. 2. (Color online) (a) Calculated total density of states and partial density of states for (b) O 2*p* and (c) In 4*d*, 5*s*, and 5*p* for In_2O_3.

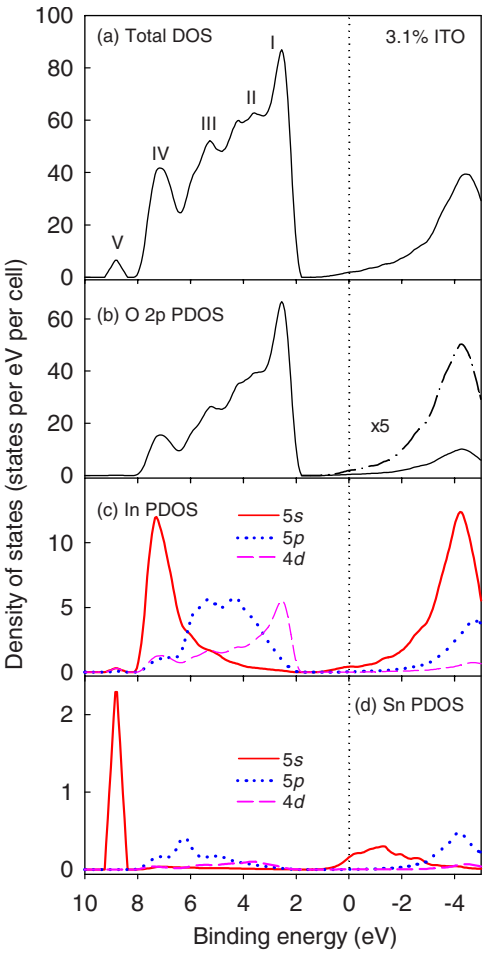

FIG. 3. (Color online) (a) Calculated total density of states and (b) partial density of states for O 2*p*, (c) In 4*d*, 5*s*, and 5*p* and (d) Sn 5*s* for 3.1% ITO.

valence band. The calculated one electron photoionization cross-sections for O 2*p*, In 4*d*, In 5*s*, and In 5*p* states, taken from the tabulations of Yeh and Lindau,[48] and from Scofield,[49] are shown in Fig. 4. It can be clearly seen that upon increasing the photon energy, the cross-section decreases for all atomic subshells. However the decrease in intensity for In 4*d*, In 5*s*, and In 5*p* orbitals is less pronounced than for the O 2*p* orbital. At higher photon energies, this has the effect of enhancing the relative intensity of O 2*p* valence-band states mixed with In 5*s*, In 5*p*, and In 4*d* states. This enhancement is proportional to the extent of the orbital hybridization. This is seen in the fact that band I, which has the most pronounced O 2*p* character, loses most intensity upon increasing the incident photon energy to 6000 eV. Conversely band IV becomes the dominant feature of the valence band because hybridization between O 2*p* and metal (In 5*s*) states is strongest at the bottom of the valence band. The strong hybridization between In 5*s* and O 2*p* states is at variance with a simple ionic model description of electronic structure which requires the valence and conduction bands to be of pure O 2*p* and In 5*s* character, respectively. At the high photon energies used in the present work, the Gelius model should provide a good basis for simulation of photoemission spectra. Figure 5 shows the total density of states for In_2O_3 and 3.1% ITO weighted with the photoionization cross sections for 1500 and 6000 eV photon energies.[49] The cross sections were corrected by a term of the form $(1+\beta/4+\gamma/2\sqrt{2}+\delta/\sqrt{2})$ where the β, γ, and δ asymmetry parameters were interpolated from the tabulations of Trzhaskovskya *et al.*[50,51] In general, taking into account the angular distribution effects, leads to some minor improvement between theory and experiment. The trends seen in the simulated spectra upon increasing the photon energy mirror those

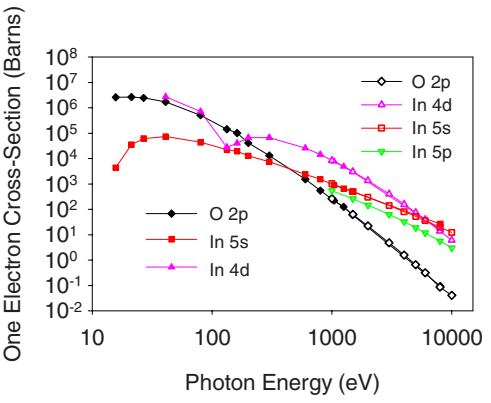

FIG. 4. (Color online) One electron photoionization cross-sections of In 4*d* (solid up-triangles), In 5*s* (solid squares) and O 2*p* (solid diamonds) orbitals as a function photon energy taken from Yeh and Lindau. (Ref. 48) One electron photoionization cross-sections of In 4*d* (hollow up-triangles), In 5*s* (hollow squares), In 5*p* (hollow down-triangles) and O 2*p* (hollow diamonds) taken from Scofield. (Ref. 49)

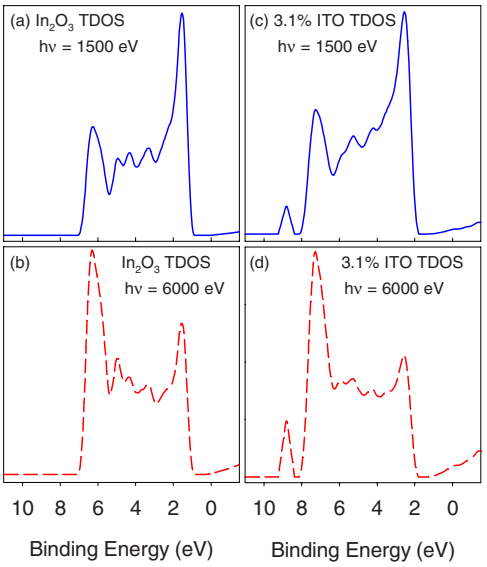

FIG. 5. (Color online) Photoionization cross-section weighted density of states of In_2O_3 at (a) 1500 and (b) 6000 eV. Photoionization cross-section weighted density of states of 3.1% ITO at (c) 1500 and (d) 6000 eV.

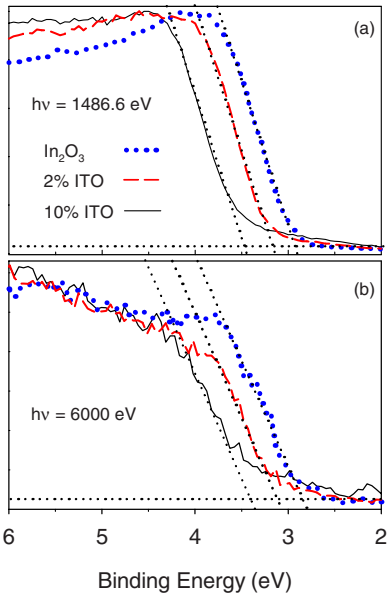

FIG. 6. (Color online) Expansions of valence band edges excited at (a) $h\nu=1486.6$ eV and (b) $h\nu=6000.0$ eV.

seen in the experiments, especially in relation to the growth in intensity of band IV as compared with the rest of the spectrum. However, quantitative agreement is not perfect and it appears that the tabulated cross sections give too high a value for the In 5*s*/O 2*p* and In 4*d*/O 2*p* cross-section ratios at 6000 eV photon energy. Similar problems have been found in comparing simulated HAXPES spectra of PbO_2 with experimental data.[15,16]

B. Conduction-band structure and spectral shifts due to doping

The Al Kα spectra shown in Fig. 1 all contain a weak peak close to the Fermi energy, terminating in a sharp Femi edge which straddles zero binding energy. This peak is associated with occupied conduction-band states. The peak grows in intensity and becomes broader with increasing carrier concentration. The conduction-band peak is also seen in spectra excited at $h\nu=6000$ eV, for both Sn-doped samples, and the intensity of this feature relative to the peak at the valence band maximium (I) is obviously higher at the higher photon energy. The differing expansions for the conduction band feature relative to the maximum intensity feature in the valence band used in Fig. 1 ($\times 5$ in HAXPES and $\times 20$ in Al Kα XPS) serve to highlight the difference in relative intensity. The intensity effects are again due to the fact that the photoionization cross section for In 5s states increases relative that for O 2*p* states with increasing photon energy. Quantitatively we find that the conduction-band maximum is eight times more intense relative to the valence band peak I for 10% ITO at $h\nu=6000$ eV, as compared with $h\nu=1486.6$ eV. Comparison with the photoionization cross section weighted partial density of states for 3.1% ITO suggests that the CBM should be five times more intense at 6000 eV. This is tolerably close to what is measured in the experimental spectrum. Somewhat surprisingly a well-defined conduction-band peak is not observed in HAXPES for the nominally undoped sample. The increasing occupancy of the conduction band with increasing carrier concentration leads to a shift in valence band features to higher binding energy. The shifts in the position of the valence-band edge for XPS and HAXPES are shown in detail in Fig. 6 and the value of the positions of the valence-band edge derived from linear fits to the experimental spectra are given in Table I.

This table also includes values for band edge positions measured for the series of samples grown on quartz and for the samples deposited on Si measured *in situ* in the deposition system. Qualitatively the shift arises because all binding energies are given relative to the Fermi energy and the Fermi level moves to increasingly higher energies within the conduction band with increasing doping. The shifts observed in photoemission spectra are closely related to the so-called Moss-Burstein shift[1,2] in optical absorption spectra. It is interesting to compare the shifts observed in XPS with those from optical absorption. As mentioned in Section II the onset of strong optical absorption increases from 3.71 eV for the nominally undoped sample with $\sigma=142$ S/cm to 4.49 eV for the most highly doped sample with $\sigma=5998$ S/cm giving an overall shift of 0.78 eV. This is in good quantitative agreement with a shift of 0.85 eV which may be extrapolated from *ab initio* calculation of In_2O_3 supercells in which 1/32, 1/64, and 1/128 of the In atoms are replaced by Sn. These calculations take full account of nonparabolicity in the conduction band as well as shrinkage or renormalization of the bulk band gap due to Sn doping.[52] The optical shift is however significantly bigger than the valence-band edge shifts obtained in the four independent series of photoemission measurements where the shifts range between 0.56 and 0.30 eV, giving an average value of 0.48 eV. This observation is consistent with pinning of the Fermi level in the nominally undoped sample by surface states that sit about 0.3 eV above

TABLE I. Optical onset energies and valence band onset energies for In_2O_3 and ITO samples.

Sample	Conductivity (S/cm)	Optical onset energy (eV)	Valence-band onset energy (eV)			
			a	b	c	d
In_2O_3	142	3.71	2.85	2.84	2.94	2.81
2% ITO	4185	4.17	3.20	3.06	3.20	3.05
10% ITO	5998	4.49	3.40	3.14	3.50	3.30

[a]measured *ex situ* with hν=1486.6 eV on samples deposited on quartz.
[b]measured *in situ* with hν=1486.6 eV on samples deposited on silicon.
[c]measured *ex situ* with hν=1486.6 eV on samples deposited on silicon.
[d]measured *ex situ* with hν=6000.0 eV on samples deposited on silicon.

the conduction band minimum: similar behavior has been found for ordered single crystal In_2O_3 surfaces with (100)[10] and (111)[53] orientation.

The carrier accumulation resulting from surface band bending will produce a space charge region whose thickness is calculated to be of the order of 5 nm.[54] The XPS signal in conventional XPS is completely dominated by the space charge region[53] but in HAXPES the longer electron mean-free path allows a significant fraction of the total valence-band signal to derive from beyond the space charge region. The differing surface sensitivities in conventional and hard XPS may account in part for the differences in relative intensity of the conduction band feature for the nominally undoped sample, as compared to the more highly doped samples. It is added however, that valence-band maximum binding energy shifts measured using *in situ* XPS often follows the shifts in optical absorption onset quantitatively.[26,55] The range of valence-band maxima of ITO thin films prepared with different carrier concentrations, i.e., by magnetron sputtering with different concentration of oxygen in the sputter gas, is 2.6–3.5 eV,[26,55–58] which is in very good agreement to the differences in absorption edge induced by different doping levels. The carrier accumulation observed at In_2O_3 surfaces might therefore be related to the particular sample preparation or processing.

C. In 3*d* core lines

The In $3d_{5/2}$ core lines measured at hν=1486.6 and 6000 eV for In_2O_3, 2% and 10% ITO are shown in Fig. 7. It should first be noted that upon increasing Sn doping levels the core level shifts to higher binding energy. This mirrors the shifts in valence-band edges discussed above.[1,2] In each case the spectra may be fitted with a pair of Voigt functions. The low binding energy component is the narrower of the two and is of dominant Gaussian character. The broader high binding energy component is dominantly Lorentzian, hinting at a broadening mechanism associated with life-time effects. Similar satellite structure has been observed before in XPS of In_2O_3 and ITO,[59] as well as other degenerately doped post-transition metal oxides such as Sb-doped SnO_2,[60,61] Tl_2O_{3-x},[62] and PbO_{2-x}.[13,16,63]

Following initial work by Kotani,[64] a model was developed by Wertheim and co-workers to describe these satellites, initially in the context of core photoemission spectra of sodium tungsten bronzes.[65–67] The Wertheim-Kotani model proposes a screening mechanism in which the Coulomb potential of the core hole at an ionized atom creates a localized trap state by pulling an orbital out of the conduction band. This is in general possible if the occupied conduction bandwidth is less than the Coulomb interaction between the core hole and the orbital contributing to the conduction band. In this situation two different final states are then accessible depending on whether the localized state remains empty (to give an unscreened final state) or is filled by transfer of an electron from the conduction band (to give a screened final state). The width of the higher binding energy unscreened state is determined by the time scale for the conduction elec-

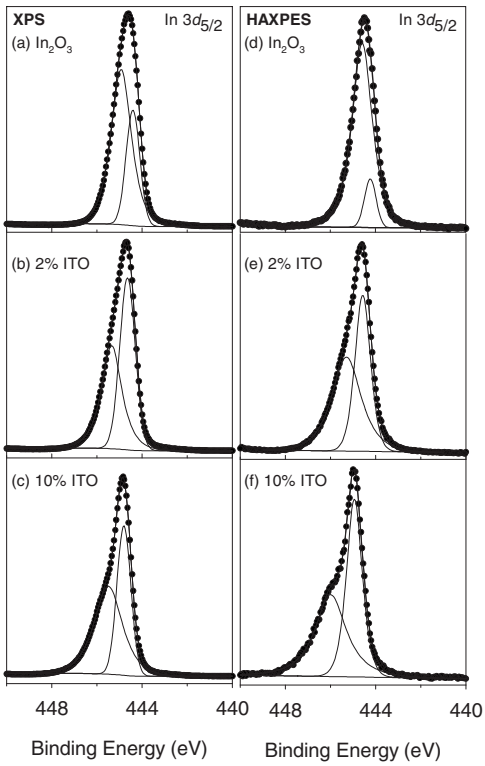

FIG. 7. In $3d_{5/2}$ core lines measured at hν=1486.6 eV (XPS) for (a) undoped In_2O_3, (b) 2% ITO and (c) 10% ITO and at hν=6000 eV (HAXPES) for (d) undoped In_2O_3, (e) 2% ITO and (f) 10% ITO.

TABLE II. Data derived by fitting In $3d_{5/2}$ core line photoemission spectra to a pair of pseudo-Voigt functions. Values of the binding energy (eV), full width at half maximum height (FWHM) (eV), Lorentzian contribution (%) and relative area (%) of the components, are given along with the satellite energy (eV), and subsequently derived carrier concentrations (cm^{-3}).

Sample	Photon energy (eV)		Binding energy (eV)	FWHM (eV)	Lorentzian contribution(%)	Relative area(%)	Satellite energy (eV)	Carrier concentration ($\times 10^{20}$ cm^{-3})
In_2O_3	1486.6	Unscreened	444.93	1.06	75	69	0.52	2.8
		Screened	444.41	0.72	7	31		
2% ITO		Unscreened	445.35	1.05	84	47	0.70	5.0
		Screened	444.65	0.81	15	53		
10% ITO		Unscreened	445.76	1.46	76	57	0.91	8.4
		Screened	444.85	0.73	3	43		
In_2O_3	6000	Unscreened	444.59	1.06	84	87	0.36	1.3
		Screened	444.23	0.61	0	13		
2% ITO		Unscreened	445.29	1.52	80	55	0.72	5.7
		Screened	444.57	0.81	51	45		
10% ITO		Unscreened	445.99	1.61	90	50	1.05	11.2
		Screened	444.94	0.82	64	50		

trons to screen the core hole. Within this model the probability of final state screening is expected to decrease as the carrier concentration decreases and in the limit of zero carrier concentration, only an unscreened final state can be reached. The relative intensity of screened and unscreened final state peaks derived by curve fitting the spectra of Fig. 7 are given in Table II. It is found that the relative intensity of the low binding energy screened final state peak does indeed decrease as the carrier concentration decreases.

A radically different model for the core line satellites is provided by a description of the high binding energy component as an unusually strong plasmon loss satellite. The Lorentzian linewidth is then determined by the conduction electron scattering rate. It was discovered early in the application of photoemission techniques to simple metallic solids that plasmon satellites make a significant contribution to core level structure in x-ray photoelectron spectra. Much of the early work in this area was concerned with unraveling the relative contributions of intrinsic and extrinsic structure and with rationalizing the pattern of multiple plasmon excitations.[68] Intrinsic plasmons arise synchronously with the creation of the core hole during the photoemission process.[69] Extrinsic plasmons are due to inelastic scattering events as the photoelectron leaves the material.[69]

The weak coupling models developed by Langreth[70] suggested that the intrinsic plasmon satellite intensity I should increase as the conduction electron density N decreases according to the expression $I \propto N^{-1/3}$. Thus within the framework of this model, the unusually high intensity of the high binding-energy satellite structure observed in the present work reflects the low density of conduction electrons. As noted above the relative intensity of the high binding energy component of the core line increases as the carrier concentration decreases, as required by the Langreth model. The present results are in accord with earlier work on Sb-doped SnO_2,[71,72] where it was found that the relative intensities of high and low binding energy components showed the $N^{-1/3}$ variation predicted by the plasmon model. It has also been shown that the plasmon energy observed in electron energy loss spectroscopy of PbO_2 is the same as the satellite energy in XPS,[63] while more recent work has established that the core XPS satellite energy for Sn-doped In_2O_3 mirrors the plasmon energy measured by infrared reflectivity. The plasmon energy $\hbar\omega_p$ is determined by the carrier concentration N through the relationship:=

$$\omega_p^2 = \frac{Ne^2}{m^* \epsilon_0 \epsilon(\infty)} \tag{1}$$

where ω_p is the plasmon frequency, m^* is the electron effective mass, ϵ_0 is the permittivity of free space and $\epsilon(\infty)$ is the optical dielectric constant. Table II shows satellite energy separations for In_2O_3, 2% and 10% ITO, respectively.

The value for the effective mass is taken to be $0.35m_0$ (Ref. 4) (where m_0 is the electron rest mass) and a dielectric constant $\epsilon(\infty)=4.0$ is assumed. Based on the core level data taken under excitation at a photon energy of 1486.6 eV the carrier concentrations are then estimated from Eq. (1) to be 2.75×10^{20}, 4.98×10^{20}, and 8.41×10^{20} cm^{-3} for undoped In_2O_3, 2% and 10% ITO respectively. The carrier concentrations calculated from plasmon energies measured under 6000 eV incident photon energy for undoped In_2O_3, 2% and 10% ITO are 1.3×10^{20}, 5.71×10^{20} and 1.12×10^{21} cm^{-3}, respectively. As stated previously, the carrier accumulation resulting from surface band bending produces a space charge region which is calculated to be about 5 nm thick. Assuming a universal curve mean free path (λ) of about 2 nm for photoelectrons with a kinetic energy close to 1.5 keV it can be shown that 97% of the photoelectron signal derives from the space charge region, as defined previously, at 45° offtake angle. Thus Al Kα photoemission is dominated by the space charge region. By contrast in HAXPES, using 6000 eV photons, λ has been estimated to be about 6 nm.[22] Now the space charge region contributes significantly less (57%) to the total photoelectron signal (measured at normal emission), with significant signal coming from the low carrier density bulk of

the sample. It is therefore expected that the screened component to the core level measured at $h\nu=6000$ eV will be weaker than when measured at $h\nu=1486.6$ eV. It is again noted that In 3*d* core levels of low conducting In_2O_3 and ITO films measured using *in situ* XPS with Al Kα excitation typically have a symmetric line shape,[26,56–58] also indicating that surface carrier accumulation is not an intrinsic feature of the material.

V. CONCLUDING REMARKS

Hard x-ray photoemission has been used in conjunction with conventional XPS and density-functional theory calculations to investigate the electronic structure of nominally undoped and Sn-doped In_2O_3. It has been found that electronic states at the bottom of the valence band and in the conduction band are enhanced relative to other spectral features in HAXPES as compared with conventional XPS. This is attributed to the fact that these states have substantial metal 5*s* character and the 5*s* photoionization cross-section decays with increasing photon energy less rapidly than the O 2*p* cross section due to the internal structure of the 5*s* radial wave function. Comparison between four independent series of photoemission measurements and optical absorption measurements provides evidence for downward band bending in the nominally undoped sample, with consequent carrier accumulation.

ACKNOWLEDGMENTS

Experimental work on transparent conducting oxides in Oxford was supported under EPSRC under grant No. GR/S94148 and the Scienta XPS facility by EPSRC under grant No. EP/E025722/1. We thank G. Beamson and D. S. L. Law for assistance with Al Kα XPS measurements. The work at NREL was funded by the U.S. Department of Energy under Contract No. DE-AC36-08GO28308. Work on the VOLPE project has been supported in part by CNR-INFM. D.J.P. is grateful to Christ Church, University of Oxford.

[1] E. Burstein, Phys. Rev. **93**, 632 (1954).
[2] T. S. Moss, Proc. Phys Soc. Sec. B **67**, 775 (1954).
[3] C. G. Granqvist and A. Hultaker, Thin Solid Films **411**, 1 (2002).
[4] I. Hamberg and C. G. Granqvist, J. Appl. Phys. **60**, R123 (1986).
[5] G. Gu, V. Bulovic, P. E. Burrows, S. R. Forrest, and M. E. Thompson, Appl. Phys. Lett. **68**, 2606 (1996).
[6] R. L. Weiher and R. P. Ley, J. Appl. Phys. **37**, 299 (1966).
[7] C. McGuinness, C. B. Stagarescu, P. J. Ryan, J. E. Downes, D. Fu, K. E. Smith, and R. G. Egdell, Phys. Rev. B **68**, 165104 (2003).
[8] P. Erhart, A. Klein, R. G. Egdell, and K. Albe, Phys. Rev. B **75**, 153205 (2007).
[9] L. F. J. Piper, A. DeMasi, S. W. Cho, K. E. Smith, F. Fuchs, F. Bechstedt, C. Körber, A. Klein, D. J. Payne, and R. G. Egdell, Appl. Phys. Lett. **94**, 022105 (2009).
[10] A. Bourlange, D. J. Payne, R. G. Egdell, J. S. Foord, P. P. Edwards, M. O. Jones, A. Schertel, P. Dobson, and J. Hutchinson, Appl. Phys. Lett. **92**, 092117 (2008).
[11] A. Walsh, J. Da Silva, S.-H. Wei, C. Körber, A. Klein, L. Piper, A. DeMasi, K. E. Smith, G. Panaccione, P. Torelli, D. J. Payne, A. Bourlange, and R. G. Egdell, Phys. Rev. Lett. **100**, 167402 (2008).
[12] D. J. Payne, R. G. Egdell, A. Walsh, G. W. Watson, J. Guo, P. A. Glans, T. Learmonth, and K. E. Smith, Phys. Rev. Lett. **96**, 157403 (2006).
[13] D. J. Payne, R. G. Egdell, D. S. L. Law, P. A. Glans, T. Learmonth, K. E. Smith, J. H. Guo, A. Walsh, and G. W. Watson, J. Mater. Chem. **17**, 267 (2007).
[14] A. Walsh, G. W. Watson, D. J. Payne, R. G. Edgell, J. Guo, P. A. Glans, T. Learmonth, and K. E. Smith, Phys. Rev. B **73**, 235104 (2006).
[15] D. J. Payne, R. G. Egdell, G. Paolicelli, F. Offi, G. Panaccione, P. Lacovig, G. Monaco, G. Vanko, A. Walsh, G. W. Watson, J. Guo, G. Beamson, P. A. Glans, T. Learmonth, and K. E. Smith, Phys. Rev. B **75**, 153102 (2007).
[16] D. J. Payne, G. Paolicelli, F. Offi, G. Panaccione, P. Lacovig, G. Beamson, A. Fondacaro, G. Monaco, G. Vanko, and R. G. Egdell, J. Electron Spectrosc. Relat. Phenom. **169**, 26 (2009).
[17] E. Papalazarou, M. Gatti, M. Marsi, V. Brouet, F. Iori, L. Reining, E. Annese, I. Vobornik, F. Offi, A. Fondacaro, S. Huotari, P. Lacovig, O. Tjernberg, N. B. Brookes, M. Sacchi, P. Metcalf, and G. Panaccione, Phys. Rev. B **80**, 155115 (2009).
[18] W. Drube, Nucl. Instrum. Methods Phys. Res. A **547**, 87 (2005).
[19] C. S. Fadley, Nucl. Instrum. Methods Phys. Res. A **547**, 24 (2005).
[20] S. Hüfner, S. Schmidt, and F. Reinert, Nucl. Instrum. Methods Phys. Res. A **547**, 8 (2005).
[21] K. Siegbahn, Nucl. Instrum. Methods Phys. Res. A **547**, 1 (2005).
[22] M. Sacchi, F. Offi, P. Torelli, A. Fondacaro, C. Spezzani, M. Cautero, G. Cautero, S. Huotari, M. Grioni, R. Delaunay, M. Fabrizioli, G. Vanko, G. Monaco, G. Paolicelli, G. Stefani, and G. Panaccione, Phys. Rev. B **71**, 155117 (2005).
[23] K. Kobayashi, M. Yabashi, Y. Takata, T. Tokushima, S. Shin, K. Tamasaku, D. Miwa, T. Ishikawa, T. Nohira, H. Hattori, Y. Sugita, O. Nakatsuka, A. Sakai, and S. Zaima, Appl. Phys. Lett. **83**, 1005 (2003).
[24] H. Sato, K. Shimada, M. Arita, K. Hiraoka, K. Kojima, Y. Takeda, K. Yoshikawa, M. Sawada, M. Nakatake, H. Namatame, M. Taniguchi, Y. Takata, E. Ikenaga, S. Shin, K. Kobayashi, K. Tamasaku, Y. Nishino, D. Miwa, M. Yabashi, and T. Ishikawa, Phys. Rev. Lett. **93**, 246404 (2004).
[25] A. Yamasaki, S. Imada, H. Higashimichi, H. Fujiwara, T. Saita, T. Miyamachi, A. Sekiyama, H. Sugawara, D. Kikuchi, H. Sato, A. Higashiya, M. Yabashi, K. Tamasaku, D. Miwa, T. Ishikawa, and S. Suga, Phys. Rev. Lett. **98**, 156402 (2007).
[26] Y. Gassenbauer and A. Klein, Solid State Ion. **173**, 141 (2004).
[27] H. Hartnagel, A. Dewar, A. Jain, and C. Jagadish, *Semiconducting Transparent Thin Films* (Institute of Physics Publishing,

Bristol, 1995).
[28] D. Ensling, A. Thissen, Y. Gassenbauer, A. Klein, and W. Jaegermann, Adv. Eng. Mater. **7**, 945 (2005).
[29] G. Paolicelli, A. Fondacaro, F. Offi, G. Stefani, G. Cautero, M. Cautero, B. Krastanov, P. Lacovig, P. Pittana, R. Sergo, R. Tommasini, P. Torelli, M. Sacchi, M. Grioni, G. Monaco, and G. Panaccione, J. Electron Spectrosc. Relat. Phenom. **144**, 963 (2005).
[30] G. Panaccione, G. Cautero, A. Fondacaro, M. Grioni, P. Lacovig, G. Monaco, F. Offi, G. Paolicelli, M. Sacchi, G. Stefani, and P. Torelli, Nucl. Instrum. Methods Phys. Res. A **547**, 56 (2005).
[31] P. Torelli, M. Sacchi, G. Cautero, M. Cautero, B. Krastanov, P. Lacovig, P. Pittana, R. Sergo, R. Tommasini, A. Fondacaro, F. Offi, G. Paolicelli, G. Stefani, M. Grioni, R. Verbeni, G. Monaco, and G. Panaccione, Rev. Sci. Instrum. **76**, 023909 (2005).
[32] W. Kohn and L. Sham, Phys. Rev. **140**, A1133 (1965).
[33] P. Hohenberg and W. Kohn, Phys. Rev. **136**, B864 (1964).
[34] P. E. Blöchl, Phys. Rev. B **50**, 17953 (1994).
[35] G. Kresse and J. Furthmüller, Phys. Rev. B **54**, 11169 (1996).
[36] G. Kresse and J. Furthmüller, Comput. Mater. Sci. **6**, 15 (1996).
[37] J. P. Perdew, K. Burke, and M. Ernzerhof, Phys. Rev. Lett. **77**, 3865 (1996).
[38] M. Marezio, Acta Crystallogr. **20**, 723 (1966).
[39] H. Monkhorst and J. Pack, Phys. Rev. B **13**, 5188 (1976).
[40] A. Walsh, J. L. F. Da Silva, and S. H. Wei, Phys. Rev. B **78**, 075211 (2008).
[41] M. Marsman, J. Paier, A. Stroppa, and G. Kresse, J. Phys.: Condens. Matter **20**, 064201 (2008).
[42] J. Paier, M. Marsman, K. Hummer, G. Kresse, I. Gerber, and J. Angyan, J. Chem. Phys. **124**, 154709 (2006).
[43] J. Heyd and G. Scuseria, J. Chem. Phys. **121**, 1187 (2004).
[44] J. Heyd, G. Scuseria, and M. Ernzerhof, J. Chem. Phys. **118**, 8207 (2003).
[45] A. Walsh, J. L. F. Da Silva, Y. Yan, M. M. Al-Jassim, and S. H. Wei, Phys. Rev. B **79**, 073105 (2009).
[46] F. Fuchs and F. Bechstedt, Phys. Rev. B **77**, 155107 (2008).
[47] K. Nomura, Y. Ujihira, S. Tanaka, and K. Matsumoto, Hyperfine Interact. **42**, 1207 (1988).
[48] J. J. Yeh and I. Lindau, At. Data Nucl. Data Tables **32**, 1 (1985).
[49] J. Scofield, Lawrence Livermore National Laboratory, Report No. UCRL-51326, 1973 (unpublished).
[50] M. B. Trzhaskovskaya, V. K. Nikulin, V. I. Nefedov, and V. G. Yarzhemsky, At. Data Nucl. Data Tables **92**, 245 (2006).
[51] M. B. Trzhaskovskaya, V. I. Nefedov, and V. G. Yarzhemsky, At. Data Nucl. Data Tables **77**, 97 (2001).
[52] I. Hamberg, C. G. Granqvist, K. F. Berggren, B. E. Sernelius, and L. Engstrom, Phys. Rev. B **30**, 3240 (1984).
[53] K. Zhang, D. Payne, R. Palgrave, V. Lazarov, W. Chen, A. Wee, C. McConville, P. King, T. Veal, G. Panaccione, P. Lacovig, and R. G. Egdell, Chem. Mater. **21**, 4353 (2009).
[54] P. D. C. King, T. D. Veal, D. J. Payne, A. Bourlange, R. G. Egdell, and C. F. McConville, Phys. Rev. Lett. **101**, 116808 (2008).
[55] A. Klein, C. Körber, A. Wachau, F. Suuberlich, Y. Gassenbauer, R. Schafranek, S. Harvey, and T. Mason, Thin Solid Films **518**, 1197 (2009).
[56] Y. Gassenbauer, R. Schafranek, A. Klein, S. Zafeiratos, M. Havecker, A. Knop-Gericke, and R. Schlogl, Phys. Rev. B **73**, 245312 (2006).
[57] Y. Gassenbauer and A. Klein, J. Phys. Chem. B **110**, 4793 (2006).
[58] S. P. Harvey, T. O. Mason, Y. Gassenbauer, R. Schafranek, and A. Klein, J. Phys. D **39**, 3959 (2006).
[59] V. Christou, M. Etchells, O. Renault, P. J. Dobson, O. V. Salata, G. Beamson, and R. G. Egdell, J. Appl. Phys. **88**, 5180 (2000).
[60] R. G. Egdell, W. R. Flavell, and P. Tavener, J. Solid State Chem. **51**, 345 (1984).
[61] R. G. Egdell, J. Rebane, T. J. Walker, and D. S. L. Law, Phys. Rev. B **59**, 1792 (1999).
[62] P. A. Glans, T. Learmonth, K. E. Smith, J. Guo, A. Walsh, G. W. Watson, F. Terzi, and R. G. Egdell, Phys. Rev. B **71**, 235109 (2005).
[63] D. J. Payne, R. G. Egdell, W. Hao, J. S. Foord, A. Walsh, and G. W. Watson, Chem. Phys. Lett. **411**, 181 (2005).
[64] A. Kotani and Y. Toyozawa, J. Phys. Soc. Jpn. **37**, 912 (1974).
[65] M. Campagna, G. K. Wertheim, H. R. Shanks, F. Zumsteg, and E. Banks, Phys. Rev. Lett. **34**, 738 (1975).
[66] J. N. Chazalviel, M. Campagna, G. K. Wertheim, and H. R. Shanks, Phys. Rev. B **16**, 697 (1977).
[67] G. K. Wertheim, Chem. Phys. Lett. **65**, 377 (1979).
[68] P. Steiner, H. Hochst, and S. Hufner, *Photoemission in Solids II* (Springer-Verlag, Berlin, 1979), Vol. 26.
[69] J. J. Chang and D. C. Langreth, Phys. Rev. B **8**, 4638 (1973).
[70] D. C. Langreth, *Proceedings of Nobel Symposium 24 in Medicine and Natural Science*, edited by B. Lundqvist and S. Lundqvist (Academic Press, New York and London, 1973), p. 210.
[71] P. A. Cox, R. G. Egdell, C. Harding, A. F. Orchard, W. R. Patterson, and P. J. Tavener, Solid State Commun. **44**, 837 (1982).
[72] R. G. Egdell, T. J. Walker, and G. Beamson, J. Electron Spectrosc. Relat. Phenom. **128**, 59 (2003).